Journal of Renewable Energy and Environment

Research Article

Journal Homepage: www.jree.ir

Multi-Objective Optimization of the Humidification-Dehumidification Desalination System for Productivity and Size

Amir Reza Khedmati, Mohammad Behshad Shafii*

Department of Mechanical Engineering, Sharif University of Technology, Tehran, Iran.

PAPER INFO

Paper history:
Received 31 October 2019
Accepted in revised form 29 February 2020

Keywords:
Humidification-Dehumidification
Desalination
Gained Output Ratio
Multi-Objective
Optimization

ABSTRACT

The humidification-dehumidification system is one of the desalination technologies that can utilize non-fossil thermal sources and requires insignificant input energy. This system is usually suitable for rural areas and places far from the main sources of energy. The purpose of this study is to obtain the most suitable working conditions and dimensions of this system. In this research, thermodynamic modeling was first performed for a simple type of the system (water-heated); then, the effect of parameters on the system performance was investigated. Modeling was conducted through a numerical simulation; furthermore, the assumption of the saturation of exhaust air from the humidifier was also considered in the mentioned code. Afterward, a comparison was made between two different forms of the system, and the proper form was chosen for the rest of the research. Moreover, through heat transfer equations, the dimensions of the two main parts of the system, i.e., humidifier and dehumidifier, were calculated. Besides, multi-objective optimization was carried out for two objective functions, i.e., gained output ratio (GOR) and the system volume, to reduce the space occupied by the system and reach the desired efficiency simultaneously. The optimization was performed using a simulation program, and results were obtained for different weights in order to optimize each objective function. For instance, 379 liters of freshwater can be produced in a day with a total volume of 48 liters for the humidifier and the dehumidifier in the optimized system.

1. INTRODUCTION

The daily and rapid reduction of drinking water is one of the concerning problems worldwide. The entire water resources of the earth are about 1.4 billion cubic kilometers, of which 97.5 % is in the oceans and only 2.5 % is in the atmosphere, aquifers, and polar ice. Then, 0.014 % of all water reservoirs are directly accessible [2].

For this reason, the ability to implement water desalination systems is becoming more and more critical. Among such systems are the multi-effect distillation system, the multi-stage flash distillation system, and the reverse osmosis system as some common types. However, these systems use fossil fuels or high-exergy sources. For this reason, other types of desalination systems, which use renewable energies, will be further discussed by the scientific community in the future. In addition to the above, the high capital and operational expenses of these systems led us to launch systems such as the humidification-dehumidification desalination system for remote and low population areas.

The humidification-dehumidification desalination system is of various types: closed air-open water and closed water-open air [2]. Typically, these systems comprise three essential parts: humidifier, heater, and dehumidifier. First, seawater penetrates the low-temperature cooling coil. In this step, seawater is pre-heated with humid air, as shown in Figure 1, in order to increase the efficiency of the whole system. In the heater (e.g., a solar collector), the intake water absorbs the heat necessary for evaporation after pre-heating. In the humidifier, the hot water blows out from the spray after being heated in a heater (the heat source); brine drips out from the bottom of this compartment, and water droplets humidify the dry air. Eventually, in the dehumidifier, water vapor in the humidified air condenses through the reaction between heat and water entering from the sea and is removed from the bottom of the compartment. In Figure 1, one can see a sample of an HDH system.

Hou et al. [3] investigated the function of a solar humidification-dehumidification desalination system using the pinch method. At specified temperatures of spraying and cooling water, they found that there was an optimum mass flow rate ratio of water to dry air to maximize the thermal energy recovery ratio. It is also noted that, for minimum temperature differences at pinches (1 °C), HDH could reach 0.75 for the energy recovery ratio; however, the heat exchanger area would probably increase.

He et al. [4,5] studied the water-heated CAOW-HDH theoretically, where the waste exhaust gas from a furnace was the heat source. They analyzed the mentioned system in terms of cost and selected both humidifier and dehumidifier as packed-bed. The final results of GOR and productivity were found to be 1.44 and 84.60 kg/h, respectively. He et al. [6] investigated an air-heated CAOW-HDH from thermodynamic and economic perspectives, where the system is composed of a packed-bed humidifier, a plate-type dehumidifier, and a waste heat recovery exchanger. Zubair et al. [7] used ETC with heat pipes as a heat source for their water-heated CAOW-HDH system. For this system, thermo-economic considerations and optimization analyses were carried out in four different geographical areas.

Niroomand et al. [8] theoretically investigated an OAOW-HDH (open air-open water), where the dehumidifier is a direct contact type. They reported that the higher production of

*Corresponding Author's Email: behshad@sharif.edu (M.B. Shafii)

freshwater could be reached by raising the flow rate and temperature of hot water and lowering the two former parameters for cold water. Dehghani et al. [9] experimentally studied a water-heated OAOW-HDH with a packed-bed humidifier and a direct contact dehumidifier. A gas burner heater was chosen as the heat source. It should be noted that brine recirculation was studied to reduce adverse effects on the environment. They found that raising the salinity of the recirculated brine could increase the overall recovery ratio of the system. Moreover, a productivity rate of 49 kg/h for was achieved in the mentioned study.

Elminshawy et al. [10,5] used a solar still with reflectors as the humidifier, a shell, and a tube heat exchanger as the dehumidifier and electrical water heaters as the heat source for a novel water-heated OACW-HDH. The productivity of the freshwater increased by 366 % because of the immersed water heaters and an external reflector.

Gang et al. [11] applied a three-stage packed-bed system as a humidifier in order to reach a higher contact surface. They achieved a value of 182.47 kg/h for freshwater productivity.

Yıldırım and Solmuş [12] used a packed-bed humidifier with FPC heat sources of different configurations of the water/air-heated OACW-HDH system. They found the optimum values of the air mass flow rate and the inclination angle of FPCs. Rajaseenivasan and Srithar [13] investigated the OACW-HDH system with a special FPC, where both water and air were heated simultaneously [5]; then, air passed over the upper surface of the absorber plate and water crossed the riser tubes at the bottom of the absorber plate. The result showed 15.23 kg.day/m^2 productivity for freshwater. Deniz and Çınar [14] studied and tested a novel OACW-HDH solar system from exergy, economic, and environmental points of view. They found the amount of 1117.3 g/h for the maximum freshwater production rate and 0.0981 USD/L for the estimated cost of freshwater produced.

The present research focuses on minimizing the volume of a simple water-heated CAOW-HDH system while maximizing its efficiency. A thorough review of the literature revealed no such study with the objectives mentioned earlier on particular types of the humidifier (i.e., packed-bed) and dehumidifier (i.e., helical coil heat exchanger). The humidifier and dehumidifier used in this research have proper contact surface for the humidifying mechanism and the appropriate mixing mechanism for better heat transfer, respectively. Moreover, this research aims to find useful decision variables on the GOR and size of the system. New parameters such as coil diameter in the dehumidifier, velocity of air circulation in the dehumidifier, and some other parameters are the strengths of this study.

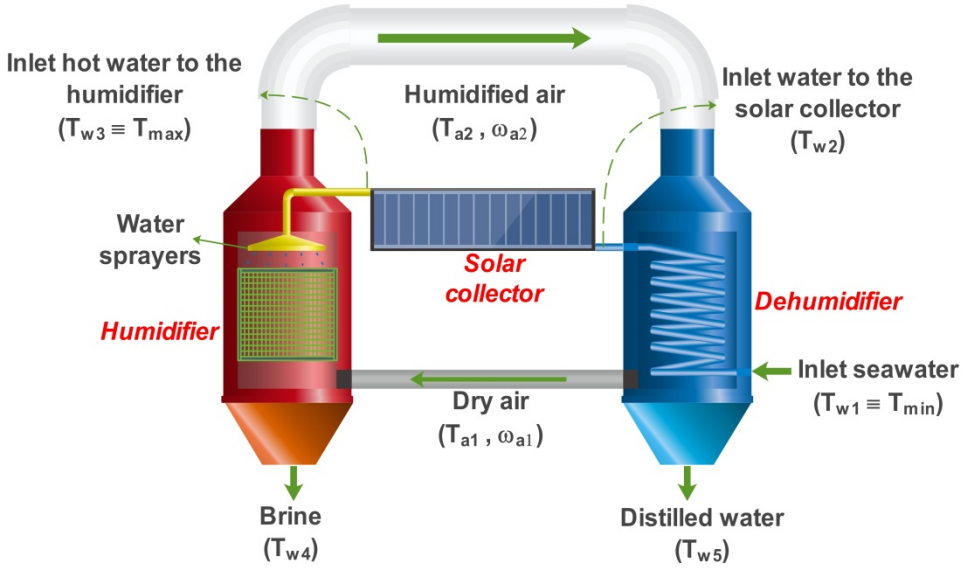

Figure 1. Schematic of a CAOW-HDH system.

2. MATERIALS AND METHOD

2.1. Thermodynamic modeling

In order to model the system in the simple form (closed air-open water), the mass-conservation, energy conservation, and second law of thermodynamics equations were written for all three parts of the system, i.e., humidifier, dehumidifier, and heater. In the simple model of the system, water is drawn from the sea and a steady stream of air circulates in the cycle. Equations for the humidifier are written below:

$$\dot{m}_{w1} - \dot{m}_{w4} = \dot{m}_{da} \times (\omega_{a2} - \omega_{a1}) \quad (1)$$

$$\dot{m}_{w1} \times h_{w3} - \dot{m}_{w4} \times h_{w4} = \dot{m}_{da} \times (h_{a2} - h_{a1}) \quad (2)$$

$$\dot{m}_{w4} \times s_{w3} - \dot{m}_{w1} \times s_{w3} + \dot{m}_{da} \times (s_{a2} - s_{a1}) = \dot{S}_{gen,h} \quad (3)$$

Similar to Equations 1-3, there are three equations for the dehumidifier, which are recognized by (4-6):

$$\dot{m}_{da} \times (\omega_{a2} - \omega_{a1}) = \dot{m}_{w5} \quad (4)$$

$$\dot{m}_{w1} \times h_{w3} - \dot{m}_{w4} \times h_{w4} = \dot{m}_{da} \times (h_{a2} - h_{a1}) \quad (5)$$

$$\dot{m}_{w4} \times s_{w3} - \dot{m}_{w1} \times s_{w3} + \dot{m}_{da} \times (s_{a2} - s_{a1}) = \dot{S}_{gen,h} \quad (6)$$

In addition, Equations 7 and 8 are written for the heater section:

$$\dot{m}_{w1} \times (h_{w3} - h_{w2}) = \dot{Q}_{in} \quad (7)$$

$$\dot{m}_{w1} \times (s_{w3} - s_{w2}) = \dot{S}_{gen,HS} \quad (8)$$

In this case, there are eight equations and ten unknowns, according to the data shown in Table 1 [1].

Table 1. Input data for the verification of the numerical simulation [1].

Variable (unit)	Value
T_{min} (°C)	30
T_{max} (°C)	80
e_h (-)	0.8
e_d (-)	0.7
φ_{a1}	1
φ_{a2}	1
S (ppm)	35000

It should be noted that T_5 is assumed to be the average of the inlet and outlet air temperatures of the humidifier (or dehumidifier) [1]. Further, T_1,T_3 are the minimum and maximum temperatures in the cycle, respectively. Therefore, two auxiliary equations, i.e., the effectiveness of the two heat exchangers, are used in the following to accommodate solving the equations simultaneously [15]. These equations were added to not only solve the thermodynamic modeling equations, but also prepare the simulation for heat transfer modeling in the upcoming section (i.e., Section 2.4).

$$e_1 = \frac{\dot{m}_{w1}\times h_{w3} - \dot{m}_{w4}\times h_{w4}}{\dot{m}_{w1}\times h_{w3} - \dot{m}_{w4}\times h_{w4,ideal}} \quad (9)$$

$$e_2 = \frac{\dot{m}_{w5}\times (h_{a2} - h_{a1})}{\dot{m}_{w5}\times (h_{a2.ideal} - h_{a1})} \quad (10)$$

$$e_h = \max(e_1, e_2) \quad (11)$$

$$e_3 = \frac{h_{w1} - h_{w2}}{h_{w1} - h_{w2,ideal}} \quad (12)$$

$$e_4 = \frac{h_{a1} - h_{a2}}{h_{a1.ideal} - h_{a2}} \quad (13)$$

$$e_d = \max(e_3, e_4) \quad (14)$$

where the first triple equations are for the humidifier and the rest for the dehumidifier. Note that the subscript ideal refers to the same condition (i.e., temperature) of the other inlet flow (e.g., inlet air) for the mentioned flow (e.g., inlet water) in the heat exchanger (i.e., the humidifier or dehumidifier).

The results of the verification of the simulation program are shown in Figure 2, in which GOR is the enthalpy ratio of evaporation of the produced freshwater to the input heat. Note that Figure 2 shows the same inputs used in Ref. [1]. This input data is shown in Table 1. A relative error of 2.38 % can be observed in the present work, which is acceptable. Moreover, the mass flow rate ratio was observed to have an optimum point for GOR due to the lower and upper bounds of the mass flow rate ratio; if the amount of water circulating in the system is much more than the air inside it, the air cannot carry much water. On the contrary, if the amount of air circulating in the cycle is much more than the water inside it, lower freshwater is made. It should be noted that the number of iterations, relative residuals, and the change in variables were fixed on 250, 1E-06, and 1E-09, respectively.

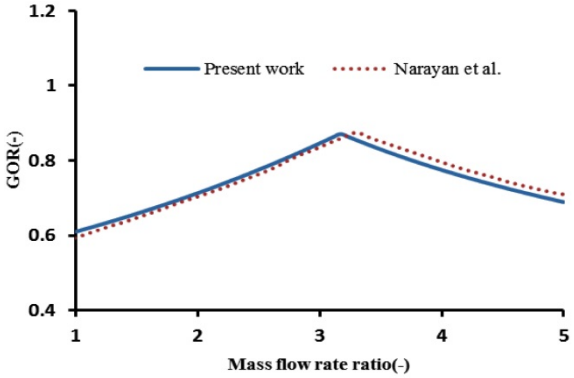

Figure 2. Verification of the simulation program.

Table 2. Input data for parametric study of a CAOW-HDH [1] (In each plot taken, one input data variable and the rest follow this table).

Variable (unit)	Value
T_{min} (°C)	35
T_{max} (°C)	80
e_h (-)	0.9
e_d (-)	0.9
φ_{a1}	1
φ_{a2}	1
S (ppm)	35000

2.2. Parametric study: Effect of input variables on GOR

Higher GOR is the reason for the higher efficiency of the overall system, yet with lower system irreversibility [1]. For this reason, the effect of input variables on GOR is evaluated. The input variables include the minimum temperature (i.e., the seawater inlet temperature), the maximum temperature (i.e., the temperature of the output water from the heater), and the effectiveness of the humidifier and the dehumidifier. To determine the effect of these inputs, in each step, one of them was selected to be a variable and the rest were kept constant. The base case data are shown in Table 2 [1]. In this case, the most effective variable is the effectiveness of the dehumidifier, which indicates the importance of this heat exchanger. For instance, the effects of three variables on GOR are discussed here (Figures 3, 4, and 5):

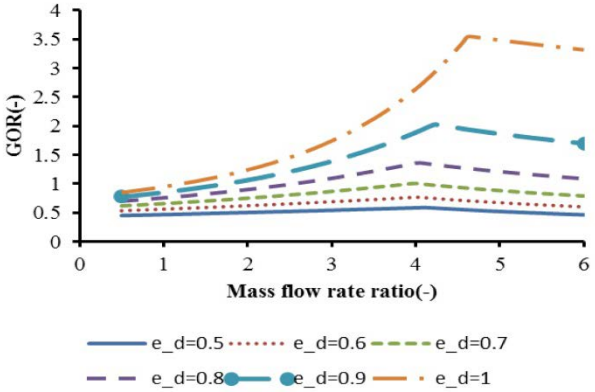

Figure 3. Effect of the dehumidifier on GOR.

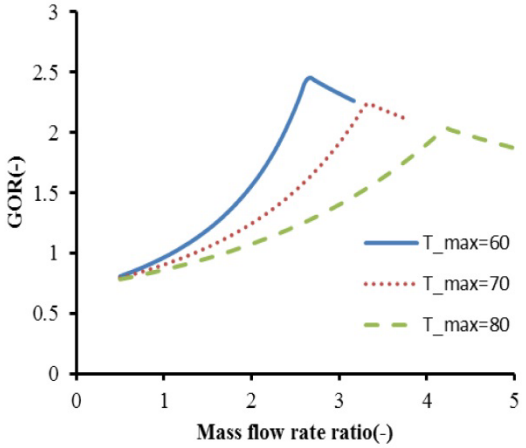

Figure 4. Effect of the maximum temperature on GOR.

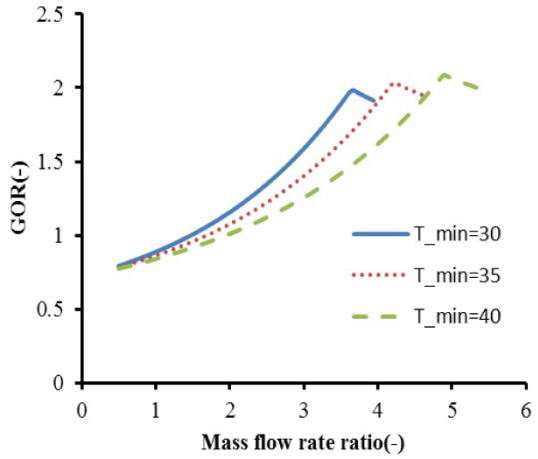

Figure 5. Effect of the minimum temperature on GOR.

As shown in Figure 3, the higher effectiveness of the dehumidifier resulted in higher GOR. Accordingly, changing the effectiveness from 0.9 to 1 (ideal) resulted in a considerable increase by 79 % for the maximum GOR (from 1.975 to 3.539). This phenomenon is evident because the function of the dehumidifier grew obviously. It should be noted that the mass flow rate ratio did not change regularly. Moreover, as demonstrated in Figure 4, the higher maximum temperature resulted in lower GOR. Accordingly, changing the maximum temperature from 70 to 80 ℃ resulted in a 16 % decrease in the maximum GOR (from 2.211 to 1.905). According to Figure 5, the higher minimum temperature resulted in higher GOR. On this basis, changing the minimum temperature from 30 to 35 ℃ resulted in a 4.2 % increase in the maximum GOR (from 1.929 to 2.011).

Furthermore, by comparing the effects of the minimum and maximum temperatures on GOR, it was observed that approaching the high and low temperatures of the cycle increased GOR and lowered its irreversibility, respectively. Furthermore, the effectiveness of the dehumidifier was higher than that of the humidifier.

2.3. Comparison of water-heated and air-heated types

In the air-heated type, the air is replaced by water only in the heater section. Note that if the air was heated before the humidifier, the heat given to the brine from the heated air would be dissipated (if there was no brine-recycling); thus, the air should be heated only after the humidifying process. Of course, the relative humidity of the outlet air from the heater was also added to the unknowns of the system; thus, this parameter was optimized for the air-heated type to find the maximum GOR. In this case, for the given data in Table 3 [1], the maximum GOR was found. It was observed that the maximum amount of GOR in the air-heated type was about 17 % more than that in the other type. Of course, due to the lack of temperature stability in the air-heated type system and its rigidity (e.g., for initial variant data in the system such as a change in the seawater temperature), this system is not highly functional (due to the lower heat capacity of air than water). For this reason, optimization was performed for the water-heated type in further sections in this research.

Table 3. Input data for a comparison of two types of HDH [1].

Variable (unit)	Value
T_{min} (°C)	35
T_{max} (°C)	80
e_h (-)	0.9
e_d (-)	0.9
φ_{a1}	1
φ_{a2}	1
S (ppm)	35000

2.4. Heat transfer modeling

The volume of the desalination system is calculated through heat transfer equations. In this case, the size of the heating section (heater) is not considered, and the other two (humidifier and dehumidifier) are evaluated. A helical coil heat exchanger was used to successfully reduce the volume of the system for the dehumidifier part. This heat exchanger is suitable for low fluxes, unlike shell and tube heat exchangers. Moreover, a packed-bed system is used for air humidification, which has a good contact surface for humidifying the air. As a result, the final system is compact and small in size.

2.4.1. Dehumidifier

2.4.1.1. Shell side equations

The equivalent diameter for this part is determined through Equation 15:

$$D_{eq}=\sqrt{\frac{4\dot{m}_s}{\pi\times\rho\times u_s}} \quad (15)$$

In addition, Reynolds and Prandtl's numbers are defined through Equations 16 and 17:

$$Re=\frac{\rho\times u_s\times D_{eq}}{\mu} \quad (16)$$

$$Pr=\frac{\mu\times C_p}{k} \quad (17)$$

Nusselt number and heat transfer coefficient in turbulent flows are evaluated by Equations 18 and 19 [16]:

$$Nu=0.023\times Re^{0.8}\times Pr^{0.4} \quad (18)$$

$$h=\frac{Nu\times k}{D_{eq}} \quad (19)$$

2.4.1.2. Coil side equations

Mass flow, which crosses the coil, is related to surface area and diameter of the coil by Equations 20 and 21:

$$u_c=\frac{\dot{m}_c}{\rho\times A_c} \quad (20)$$

$$A_c=(\pi/4)\times d_c^{\,2} \quad (21)$$

To determine Nusselt number and heat transfer coefficient, Equations 22 and 23 are used as follows:

$$Nu=0.023\times Re^{0.85}\times Pr^{0.4}\times(\frac{r}{R})^{0.1} \quad (22)$$

$$h=\frac{Nu\times k}{d_c} \quad (23)$$

2.4.1.3. Heat transfer analysis

The total heat transferred by the dehumidifier elements is determined through Equation 24:

$$\dot{Q}_d=U\times A\times(LMTD\times F_{helical}) \quad (24)$$

where LMTD is:

$$LMTD=\frac{(T_{s,in}-T_{c,out})-(T_{s,out}-T_{c,in})}{\ln((T_{s,in}-T_{c,out})/(T_{s,out}-T_{c,in}))} \quad (25)$$

In addition, the overall heat transfer coefficient is obtained through Equation 26:

$$\frac{1}{U}=\frac{A_e}{h_i\times A_i}+\frac{A_e\times\ln(\frac{d_e}{d_i})}{2\pi k\times L_c}+\frac{1}{h_e} \quad (26)$$

where A_e, d_e, and L_{coil} are the heat exchange area (external surface of the coil), the external diameter of the coil, and the coil length, respectively. Moreover, A_i and d_i are the internal surface and the internal diameter of the coil, respectively. Note that k is the thermal conductivity of the material used for the coil.

Remember that the effect of the centrifugal force generated by the curvature of the pipes should be taken into account. This effect is applied with a correction coefficient in the logarithmic mean temperature difference [17]:

$$F=1+3.6\times(1-\frac{r}{R})\times(\frac{r}{R})^{0.8} \quad (27)$$

Furthermore, because of the use of seawater in the coil side, one can apply Equations 28 and 24:

$$\dot{Q}_d=\dot{m}_w\times C_{p_w}\times(T_{out}-T_{in}) \quad (28)$$

Of note, the surface area for transferring heat can be calculated through Equation 29:

$$A=\pi\times d\times L_c \quad (29)$$

where L_c is the length of the coil and is related to helix radius of the coil (R) and the pitch of the coil (p) by Equation 30:

$$L_c=N\times\sqrt{(2\pi R)^2+p^2} \quad (30)$$

where the number of coils is related to the pitch by Equation 31:

$$L_s=p\times N \quad (31)$$

where L_s is the length of the shell.

The volume of the coil is determined by Equation 32:

$$V_c=(\pi/4)\times d_c^{\,2}\times L_c \quad (32)$$

The volume of the shell is obtained by Equations 33-35:

$$V_{av}=(\pi/4)\times D_{eq}\times d_e\times L_c \quad (33)$$

$$V_s=V_c+V_{av} \quad (34)$$

$$V_s=(\pi/4)\times D_s^{\,2}\times L_s \quad (35)$$

where Equation 33 is the volume available for the humidified air.

2.4.1.4. Pressure drop at shell side

To determine the pressure drop, Equations 36 and 37 are used:

$$f_s=0.184\times Re^{-0.2} \quad (36)$$

$$\Delta P=\frac{f_s\times\rho\times L_s\times u_s^{\,2}}{2D_e} \quad (37)$$

where Equation 36 is the friction factor.

2.4.1.5. Pressure drop at coil side

To obtain the pressure drop, Equations 38 and 39 are used:

$$f_c=0.046Re^{-0.2}\times\left[Re\times(\frac{r}{R})^2\right]^{0.05} \quad (38)$$

$$\Delta P=\frac{2f_c\times\rho\times L_c\times u_c^{\,2}}{d_c} \quad (39)$$

2.4.1.6. Verification of the dehumidifier model

The verification of this part was done with Ref. [16] for the preheater part of the heat exchanger mentioned in Ref. [16]. R134a refrigerant was used in the coil and the exhaust gas from the Diesel engine in the shell; Tables 4 and 5 show the initial data and results of this procedure, respectively. It could be seen that the errors are below 1 %.

Table 4. Input data for the verification of the dehumidifier model [16].

Working fluid	T inlet (K)	T outlet (K)	Pressure (kPa)
R134a	307.2	328.202	1500
Exhaust gas	487.465	403.507	200

Table 5. Verification of the dehumidifier model.

Parameter	Present model	Ref. [16]	Error (%)
Q_preheater (W)	3396	3409.52	-0.4
Shell length (m)	0.358	0.3582	-0.06

2.4.2. Humidifier

A packed-bed system has three main parts: spray zone (from spray nozzles to the surface of the packing), packing zone (consisting of the packing material), and rain zone (first part where water droplets contact with the air) [18]. It should be noted that 90 % of the heat and mass transfer occurs in the fill zone; therefore, this part is the most crucial part of this heat exchanger.

The following assumptions are reasonable to use for modeling the mentioned humidifier [18]:

- Uniform cross-sectional area for the humidifier.
- Constant pressure along with the humidifier.

It is common to use a dimensionless number called ‘’Merkel number’’ in this specific humidifier. This number is defined as follows [18]:

$$Me=\frac{h_d \times a \times V}{\dot{m}_w} \quad (40)$$

which relates the mass transfer coefficient to the effective surface area per unit volume, the volume of the humidifier, and mass flow rate of the inlet seawater. Because mass and energy balance equations for this humidifier are differential equations [18], an approximate equation for the height of the humidifier is used; thus, the optimization procedure in the upcoming sections has become possible. Moreover, the area of the humidifier is calculated through Equation (41):

$$A_h=\frac{\dot{m}_w}{flux} \quad (41)$$

where water flux is constant and assumed to be 2 $kg.m^2/s$ [18]. By combining Equation A.8 from Ref. [18] and an approximation in ε-NTU, the method for heat exchangers (Equation 11.29b from [19]), one can apply Equation 42 for the height of the humidifier.

$$H_h=\left[\frac{\ln\left(\frac{e_h-1}{e_h \times CR-1}\right)}{2.049(CR-1)\times MR^{0.221}}\right]^{\frac{1}{0.632}} \quad (42)$$

It is noted that CR is the $\min\left(\frac{MR\times C_{p_w}}{4},\frac{4}{MR\times C_{p_w}}\right)$.

The results of the approximate method are in agreement with those in [18]. For more information, check out the Appendix and [18]. Note that this equation is not almost accurate and is approximate.

2.5. Parametric study: The effect of input variables on the system dimensions

Data used in this parametric study for the system dimensions are shown in Table 6. Note that there are some technical constraints for the dimensions:

- d_e/D is chosen as 0.1 [16] as in almost all Figures; only in Figure 6, this quantity is chosen to be both 0.1 and 0.2.
- Pitch is usually set to $1.25d_e$ in heat exchangers [17].

Note that the conductivity of pure copper is used for the coil.

Table 6. Input data for the parametric study of CAOW-HDH dimensions.

Variable (unit)	Value
T_{min} (°C)	35
T_{max} (°C)	80
e_h (-)	0.9
e_d (-)	0.9
φ_{a1}	1
φ_{a2}	1
S (ppm)	35000
u_s (m/s)	5
P (kPa)	101.325
D (m)	0.2
$\dot{m}_w$ (kg/s)	0.1
T (m)	0.001
k_c (W/m.K)	386
p/d_e (-)	1.25

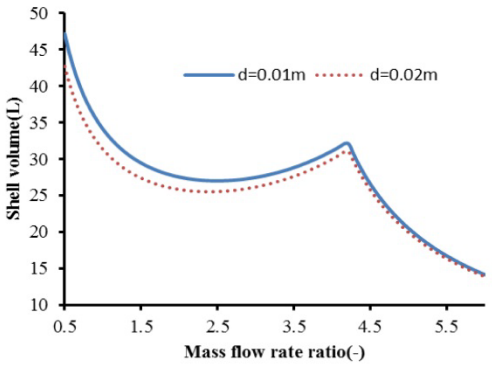

Figure 6. Effect of the inner coil diameter on the shell volume.

To determine the effect of these inputs, in each step, one of them is assumed to be a variable, and the rest are considered constant. It should be noted that only the important ones are discussed here. As shown in Figure 6, a lower inner coil diameter causes the higher volume of the dehumidifier shell. This is due to the lower overall heat transfer coefficient in this state (Equation 26). Accordingly, according to Figure 6, the volume increased from 31.02 L (d=0.02 m) to 32.13 L (d=0.01 m) at the highest GOR point in each case (a 3.5 % increase).

As shown in Figure 7, the lower maximum temperature resulted in the higher volume of the dehumidifier shell and also higher GOR, as shown in Figure 4. Moreover, these results created a two-objective optimization process (i.e., the system volume and GOR). On this basis, shell volume increased from 30.95 L (T_{max}=80 °C) to 36.57 L (T_{max}=70 °C) and 42.82 L (T_{max}=60 °C) at the highest GOR points,

which resulted in 14.6 % and 27.72 % increases in volume (relative to T_{max}=80 °C). The reason seems to be connected to the idea that lower irreversibility usually follows the area of heat transfer excess.

Moreover, for the height of the humidifier (the cross-section of the packed-bed system is constant), Figure 8 is plotted. As is shown, by increasing the effectiveness of the humidifier, the height and the volume of the system increase (as one has guessed); accordingly, changes are shown in Table 7, where there are massive changes by altering this input data. Given the effect of this parameter on GOR, one should optimize both functions simultaneously.

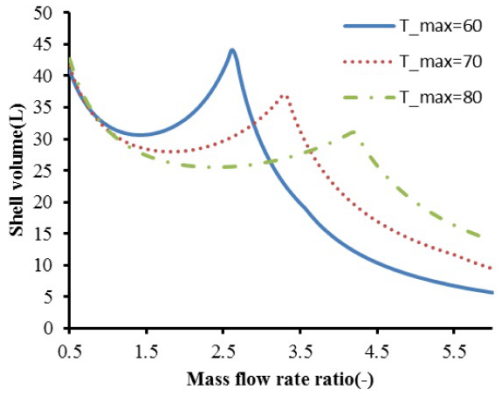

Figure 7. Effect of the maximum temperature on the shell volume (for d=0.02 m).

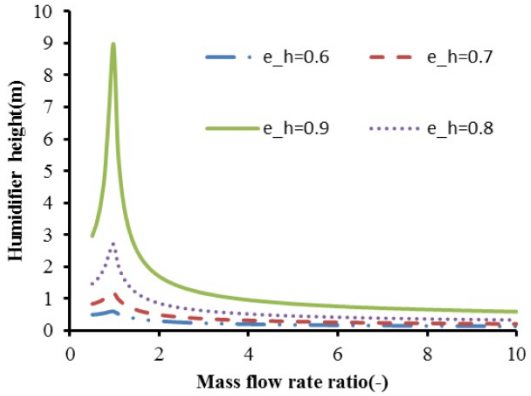

Figure 8. Effect of the humidifier on the humidifier height.

Table 7. Changes in the humidifier height with its effectiveness.

Effectiveness of humidifier	Height of humidifier (m)	Relative change (to the first case)
0.6	0.8691	-
0.7	1.009	16.1 %
0.8	2.7	210.7 %
0.9	8.96	930.9 %

In Figure 9, changing the air velocity is evaluated. As is shown, increasing this velocity caused an increase in the convection heat transfer and, consequently, a decrease in the volume of the shell. On this basis, shell volume increased from 31.02 L (u_{air}=5 m/s) to 60.66 L (u_{air}=3 m/s) and 264.2 L (u_{air}=1 m/s) at the highest GOR points; therefore, there are 95.5 % and 751.7 % relative changes to the u_{air}=5 m/s case, respectively, which are tremendous changes.

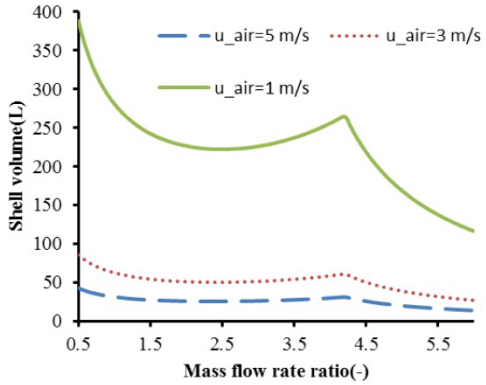

Figure 9. Effect of the air velocity on the shell volume (d=0.02 m).

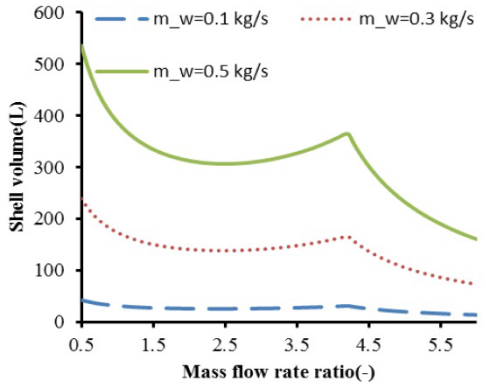

Figure 10. Effect of the mass flow rate of the seawater on the shell volume (d=0.02 m).

In Figure 10, changing the mass flow rate of the seawater is evaluated. As shown, increasing this input data extends the shell volume. Accordingly, the shell volume increased from 31.02 L ($\dot{m}_w$=0.1 kg/s) to 165.3 L ($\dot{m}_w$=0.3 kg/s) and 364.4 L ($\dot{m}_w$=0.5 kg/s) at the highest GOR points; therefore, there are 432.8 % and 1074.7 % relative change to the $\dot{m}_w$=0.1 kg/s case, respectively, which are massive changes. Thus, in this case, more amount of freshwater is produced; however, the size of the system increases (because of the rise in the area needed for heat transfer). Moreover, the allowable pressure loss in the coil section can be overshot by increasing the mass flow rate of the seawater.

3. RESULTS AND DISCUSSION

In this section, the momentous results of the previous parts are discussed in 3.1. Then, the optimization procedure and final results are presented and discussed in 3.2 and 3.3.

3.1. Key points about the useful parameters on GOR and the size of the system

- It should be noted that the last two inputs (i.e., the air velocity and the mass flow rate of the seawater) had no effects on GOR; the best quantity for each of them is set in Table 6 for optimization.
- Parametric studies for other input data can be done the same as above.
- Most essential parameters having a magnificent role in the size of the system and GOR are maximum temperature and both the effectiveness of humidifier and dehumidifier.

Table 8. Properties of the pattern search algorithm.

Property	Value
Mesh size	1
Mesh expansion factor	2
Mesh contraction factor	0.5
Max iterations	100 × number of variables
Tolerances	1e-6
Poll method	GPS positive basis 2N

3.2. Optimization procedure

The primary purpose of this article is to minimize the system volume and maximize GOR at the same time.

The pattern search optimization method was used as one of the most efficient methods for optimization [20-22]. Table 8 and Figure 11 show the properties and outline of this method, respectively.

Two objective functions were considered: GOR and the system volume. Five decision variables were selected to perform this optimization. Table 9 shows decision variables and their acceptable ranges known as constraints. Design parameters used in optimization are shown in Table 10.

One can optimize two or more objective functions by weighting each function and summing them all together in a multi-objective function. This new function is defined as follows:

$$\min (MOF = w_1 \times (-GOR) + w_2 \times TotalVolume) \qquad (43)$$

Note that the minus sign in Equation 43 is used to maximize GOR or, in other words, to minimize the negative GOR. For this purpose, six groups of weights (i.e., for w_1 and w_2) were given to the two functions, as mentioned above. These six weights, namely 90, 80, 70, 30, 20, and 10 percent for both of the objective functions with their results, are discussed in detail in the following section.

Table 9. Decision variables and their range of performance used for optimization.

Variable (unit)	Minimum value	Maximum value
T_{min} (°C)	30	40
T_{max} (°C)	60	80
e_h (-)	0.65	0.95
e_d (-)	0.65	0.95
MR (-)	0.5	6

Table 10. Design parameters for the optimization of the two functions simultaneously.

Variable (unit)	Value
φ_{a1} (-)	1
φ_{a2} (-)	1
S (ppm)	35000
u_s (m/s)	5
P (kPa)	101.325
D (m)	0.02
D (m)	0.2
$\dot{m}_w$ (kg/s)	0.1
T (m)	0.001
k_c (W/m.K)	386
p/d_e (-)	1.25
Humidifier_flux (kg.m^2/s)	2

3.3. Optimization results

Figure 12 shows a Pareto frontier curve, which was obtained to explain the conflict between the two objective functions clearer. Note that points A and B represent the least volume and the highest GOR that could be achieved, respectively. Their optimum value was 4.256 for the highest GOR and 13.12 L for the lowest volume.

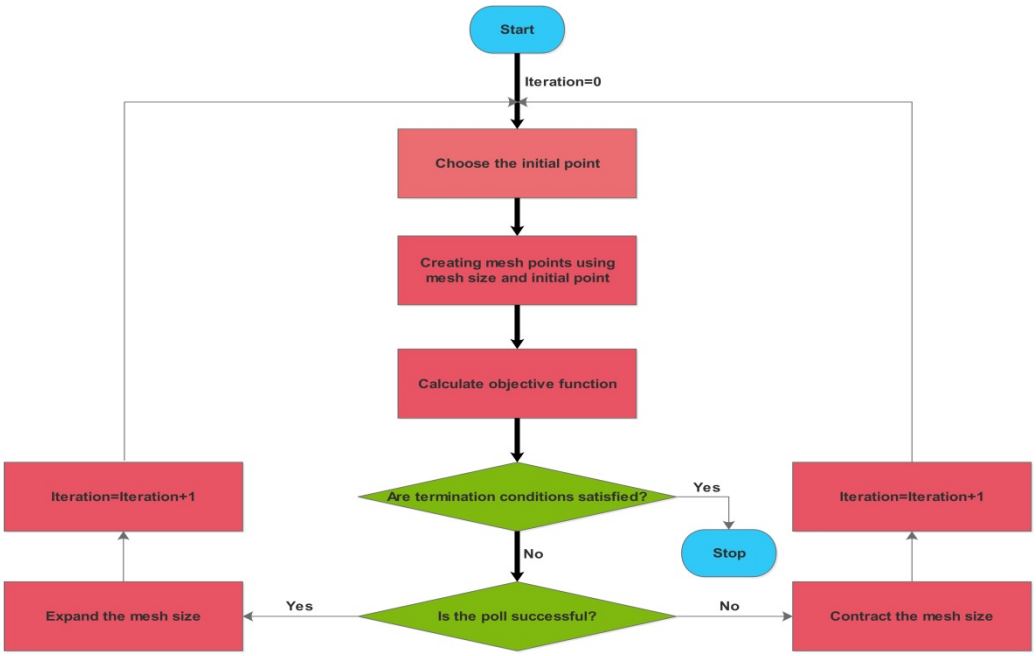

Figure 11. Flowchart of the pattern search optimization.

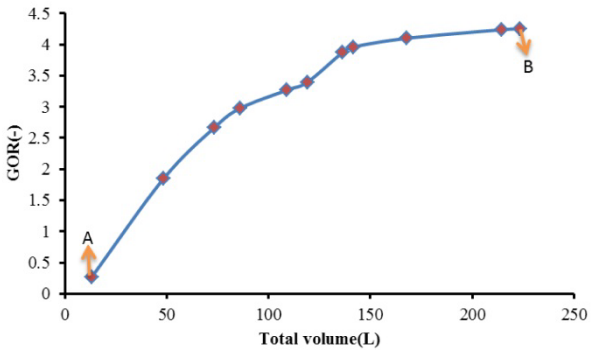

Figure 12. The Pareto curve for the objective functions.

Table 11. Optimized variables of objective functions.

Case	Weight of Volume in optimization (%)	GOR (-)	Volume (L)	Freshwater production (L/day)
1	10	4.239	214.5	216.95
2	20	4.101	167.9	216.17
3	30	3.96	141.5	215.22
4	70	2.98	86.19	303.09
5	80	2.67	73.47	336.18
6	90	1.844	48.36	379.47

Table 12. Optimized variables.

Case	T_{min} (°C)	T_{max} (°C)	e_h (-)	e_d (-)	MR (-)
1	40	60	0.95	0.95	3.162
2	40	60	0.95	0.95	3.427
3	40	60	0.95	0.95	3.722
4	39.03	70.37	0.93	0.93	5.682
5	36.5	71.81	0.91	0.93	5.900
6	30.9	74.56	0.88	0.93	5.992

According to the results of optimization shown in Tables 11 and 12, it can be seen that increasing the weight percentage of GOR caused an increase in its value; in addition, the volume of the system obviously increased. Following results were more interesting:

- Except for the mass flow rate ratio, all of the decision variables were constant at the high weights of the optimization for GOR; this means that this variable is of highest importance. The shift of the mass flow rate ratio is 6.3 % and 17.7 % compared to Case 1, resulting in 3.26 % and 6.58 % decreases in GOR (In Cases 2 and 3, respectively). Other variables are characterized by their best values to optimize GOR rather than volume.
- In Cases 4-6, other decision variables changed, too. Due to the lower effect of the minimum temperature, GOR was optimized with significant changes (6.4 % and 20.83 % for Cases 5 and 6 compared to Case 4, respectively). The maximum temperature varied at lower rates because of the results of the parametric study (Sections 2.2 and 2.5), i.e., the maximum temperature had more effects on the objective functions than the minimum temperature.
- Efficincy of the dehumidifier had significant effects as the mass flow rate ratio on the objective functions; therefore, it changed at a slow rate (in Case 6, it decreased by 1.1 % compared to Case 5). This pattern could be seen to be somewhat faster in the humidifier one (in Case 6, it decreased by 3.2 % compared to Case 5).
- At the higher weights of the optimization for GOR, higher GOR resulted in lower irreversibility and higher freshwater production; however, at the lower weights for GOR, there was higher irreversibility with higher freshwater production. This occurred because of the higher mass flow of the inlet water compared to the air (Mass flow rate ratio).

To sum up, one could find that:

- The minimum and maximum temperatures were separated from each other at lower weights of the optimization for GOR. This fact was correct based on the last part of the parametric study (Section 2.2).
- Because of the higher effects of the heat exchangers and the mass flow rate ratio, these variables could change at a lower rate; however, at least, one should change at a higher rate for producing different solutions in the optimization procedure. Fortunately, because of the ability to control the system by the mass flow rate ratio, this variable is the qualified one among them in this procedure.

Finally, a comparison between the optimized result of freshwater production (as an only objective function) and the results of previous work [23] with the same mass flows of water, air, and the maximum temperature was made, as reported in Table 13:

Table 13. Advantages of the optimization procedure.

Parameter	Present work	Dai et al. [23]
MR (-)	6.14	6.14
T_{max} (°C)	65-85	65-85
Maximum productivity (kg/h)	132	108

According to Table 13, productivity increased by 22 % in the same conditions through the optimization method, showing the advantage of the present work.

4. CONCLUSIONS

In this study, in addition to the thermodynamics and heat transfer analysis of the CAOW-HDH system, useful variables concerning the performance of the proposed system were optimized. One could find that some parameters only affected GOR (e.g., the minimum temperature) or size of the system (e.g., the mass flow rate of each flow and the air velocity in shell), while some others affected both GOR and the size of the system (e.g., the mass flow rate ratio, the maximum temperature, and effectiveness of the humidifier and dehumidifier). A Pareto frontier curve illustrated this conflict between the objective functions for optimized solutions, which were determined by choosing the weights of the multi-objective function. The highest achievable GOR was 4.239 (with 214.5 L for volume), and the lowest volume was 48.36 L (with 1.844 for GOR). The final system was small in

volume due to the type of its heat exchangers and, also, efficient due to its optimized decision variables. In addition, as a suggestion for future research, one can apply the iterative method for determining the size of the packed-bed humidifier according to the complete explanations in [9]; however, it also has to deal with the difficulties in its optimization process.

5. ACKNOWLEDGEMENT

We appreciate all the assistance and guidance that Mr. Faegh has offered to us during the course of this research.

NOMENCLATURE

A	Area
a	Effective surface area per unit volume
CR	Heat capacity ratio
C_p	Specific heat at constant pressure
D, d	Diameter
e	Effectiveness
F	Correction coefficient of heat transfer
f	Friction factor
flux	Water flux in packed-bed
H	Height of the packed-bed
h	Enthalpy (in thermodynamics), Convection heat transfer coefficient (in heat transfer)
h_d	Mass transfer coefficient
k	Thermal conductivity
L	Length
Me	Merkel number
$\dot{m}$	Mass flow rate
N	Number of coils
Nu	Nusselt number
P	Pressure
Pr	Prandtl number
p	Pitch in helical coils
$\dot{Q}$	Heat transfer rate
R	Helix radius of the helical coil heat exchanger
Re	Reynolds number
r	Internal radius of the coil of the heat exchanger
S	Salinity
s	Entropy
T	Temperature
t	Thickness of coils
U	Overall heat transfer coefficient
u	Velocity
V	Volume
w	Weight for the multi-objective optimization
Greek symbols	
μ	Dynamic viscosity
ω	Absolute humidity
φ	Relative humidity
ρ	Density
Subscripts	
in	Input
out	Output
eq	Equivalent
e	External
i	Internal
av	Available
d	Dehumidifier
da	Dry-air
gen	Generation
h	Humidifier
HS	Heat source
s	The shell of the dehumidifier
c	Coils of the dehumidifier
w	water
a1	Input air to the humidifier
a2	Output air from the humidifier
1	Inlet seawater
2	Outlet water from the dehumidifier
3	Inlet hot water to the humidifier
4	Brine
5	Freshwater produced
Abbreviations	
GOR	Gained output ratio
LMTD	Logarithmic mean temperature difference
MR	Mass flow rate ratio
MOF	Multi-objective function
NTU	Number of transfer units
HDH	Humidification dehumidification
CAOW-HDH	Closed air-open water HDH
OACW-HDH	Open air-closed water HDH
OAOW-HDH	Open air-open water HDH

APPENDICES

A. Equation A.8 from Ref. [18] is:

$$Me=2.049MR^{-0.779}\times H^{0.632} \quad (A.1)$$

where this relation is reported by the factory of Brentwood for CF1200MA Cross Fluted Film Fill Media (packing material). This equation relates the Merkel number with the mass flow rate ratio and height of the packing in meters [18].

B. Equation 11.29b from Ref. [19] is:

$$NTU=\left(\frac{1}{CR-1}\right)\times\ln\left(\frac{e-1}{e\times CR-1}\right) \quad (B.1)$$

where CR is less than one. This relation is used for counter flow heat exchangers in the ε-NTU method.

REFERENCES

1. Narayan, G.P., Sharqawy, M.H., Lienhard V.J.H. and Zubair, S.M., "Thermodynamic analysis of humidification dehumidification desalination cycles", ***Desalination and Water Treatment***, Vol. 16, No. 1-3, (2010), 339-353. (https://doi.org/10.5004/dwt.2010.1078).
2. Kabeel, A.E., Hamed, M.H., Omara, Z.M. and Sharshir, S.W., "Water desalination using a humidification-dehumidification technique—A detailed review", ***Natural Resources***, Vol. 4, No. 3, (2013), 286. (http://dx.doi.org/10.4236/nr.2013.43036).
3. Hou, S., Ye, S. and Zhang, H., "Performance optimization of solar humidification–dehumidification desalination process using Pinch technology", ***Desalination***, Vol. 183, No. 1-3, (2005), 143-149. (https://doi.org/10.1016/j.desal.2005.02.047).
4. He, W.F., Wu, F., Wen, T., Kong, Y.P. and Han, D., "Cost analysis of a humidification dehumidification desalination system with a packed bed dehumidifier", ***Energy Conversion and Management***, Vol. 171, (2018), 452-460. (https://doi.org/10.1016/j.enconman.2018.06.008).
5. Faegh, M., Behnam, P. and Shafii, M.B., "A review on recent advances in humidification-dehumidification (HDH) desalination systems integrated with refrigeration, power and desalination technologies", ***Energy Conversion and Management***, Vol. 196, (2019), 1002-1036. (https://doi.org/10.1016/j.enconman.2019.06.063).
6. He, W., Yang, H., Wen, T. and Han, D., "Thermodynamic and economic investigation of a humidification dehumidification desalination system driven by low grade waste heat", ***Energy Conversion and Management***, Vol. 183, (2019), 848-858. (https://doi.org/10.1016/j.enconman.2018.10.044).
7. Zubair, M.I., Al-Sulaiman, F.A., Antar, M.A., Al-Dini, S.A. and Ibrahim, N.I., "Performance and cost assessment of solar driven humidification dehumidification desalination system", ***Energy Conversion and Management***, Vol. 132, (2017), 28-39. (https://doi.org/10.1016/j.enconman.2016.10.005).
8. Niroomand, N., Zamen, M. and Amidpour, M., "Theoretical investigation of using a direct contact dehumidifier in humidification–dehumidification desalination unit based on an open air cycle", ***Desalination and Water Treatment***, Vol. 54, No. 2, (2015), 305-315. (https://doi.org/10.1080/19443994.2014.880157).
9. Dehghani, S., Date, A. and Akbarzadeh, A., "An experimental study of brine recirculation in humidification-dehumidification desalination of seawater", ***Case Studies in Thermal Engineering***, Vol. 14, (2019), 100463. (https://doi.org/10.1016/j.csite.2019.100463).
10. Elminshawy, N.A., Siddiqui, F.R. and Addas, M.F., "Experimental and analytical study on productivity augmentation of a novel solar

humidification–dehumidification (HDH) system", ***Desalination***, Vol. 365, (2015), 36-45. (https://doi.org/10.1016/j.desal.2015.02.019).

11. Gang, W., Zheng, H., Kang, H., Yang, Y., Cheng, P. and Chang, Z., "Experimental investigation of a multi-effect isothermal heat with tandem solar desalination system based on humidification–dehumidification processes", ***Desalination***, 378, (2016), 100-107. (https://doi.org/10.1016/j.desal.2015.09.024).
12. Yıldırım, C. and Solmuş, İ., "A parametric study on a humidification–dehumidification (HDH) desalination unit powered by solar air and water heaters", ***Energy Conversion and Management***, Vol. 86, (2014), 568-575. (https://doi.org/10.1016/j.enconman.2014.06.016).
13. Rajaseenivasan, T. and Srithar, K., "Potential of a dual purpose solar collector on humidification dehumidification desalination system", ***Desalination***, Vol. 404, (2017), 35-40. (https://doi.org/10.1016/j.desal.2016.10.015).
14. Deniz, E. and Çınar, S., "Energy, exergy, economic and environmental (4E) analysis of a solar desalination system with humidification-dehumidification", ***Energy Conversion and Management***, Vol. 126, (2016), 12-19. (https://doi.org/10.1016/j.enconman.2016.07.064).
15. Narayan, G.P. and Zubair, S.M., "Entropy generation minimization of combined heat and mass transfer devices", ***International Journal of Thermal Sciences***, Vol. 49, No. 10, (2010), 2057-2066. (https://doi.org/10.1016/j.ijthermalsci.2010.04.024).
16. Bonafoni, G. and Capata, R., "Proposed design procedure of a helical coil heat exchanger for an orc energy recovery system for vehicular application", ***Mechanics, Materials Science & Engineering Journal***, Vol. 1, (2015), 72-96. (doi:10.13140/RG.2.1.2503.5282).
17. Lazova, M., Huisseune, H., Kaya, A., Lecompte, S., Kosmadakis, G. and De Paepe, M., "Performance evaluation of a helical coil heat exchanger working under supercritical conditions in a solar organic Rankine cycle installation", ***Energies***, Vol. 9, No. 6, (2016), 432. (https://doi.org/10.3390/en9060432).
18. Sharqawy, M.H., Antar, M.A., Zubair, S.M. and Elbashir, A.M., "Optimum thermal design of humidification dehumidification desalination systems", ***Desalination***, Vol. 349, (2014), 10-21. (https://doi.org/10.1016/j.desal.2014.06.016).
19. Bergman, T.L., Incropera, F.P., DeWitt, D.P. and Lavine, A.S., Fundamentals of heat and mass transfer, ***John Wiley & Sons***, (2011).
20. Lewis, R.M., Torczon, V.J. and Kolda, T.G., "A generating set direct search augmented Lagrangian algorithm for optimization with a combination of general and linear constraints', (No. SAND2006-5315), ***Sandia National Laboratories***, (2006). (https://doi.org/10.2172/893121).
21. Conn, A.R., Gould, N.I. and Toint, P., "A globally convergent augmented Lagrangian algorithm for optimization with general constraints and simple bounds", ***SIAM Journal on Numerical Analysis***, Vol. 28, No. 2, (1991), 545-572. (https://doi.org/10.1137/0728030).
22. Conn, A., Gould, N. and Toint, P., "A globally convergent Lagrangian barrier algorithm for optimization with general inequality constraints and simple bounds", ***Mathematics of Computation of the American Mathematical Society***, Vol. 66, No. 217, (1997), 261-288. (https://doi.org/10.1090/S0025-5718-97-00777-1).
23. Dai, Y.J. and Zhang, H.F., "Experimental investigation of a solar desalination unit with humidification and dehumidification", ***Desalination***, Vol. 130, No. 2, (2000), 169-175. (https://doi.org/10.1016/S0011-9164(00)00084-9).